IEEE Photonics Journal
An IEEE Photonics Society Publication

Open Access

Multimode Fiber Coupled Superconductor Nanowire Single-Photon Detector

Volume 6, Number 5, October 2014

Labao Zhang
Ming Gu
Tao Jia
Ruiyin Xu
Chao Wan
Lin Kang
Jian Chen
Peiheng Wu

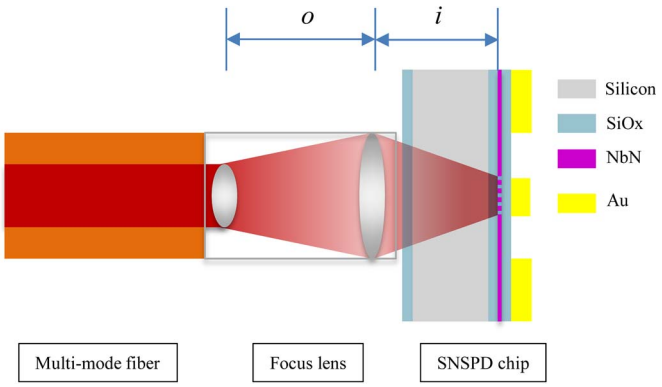

DOI: 10.1109/JPHOT.2014.2360285
1943-0655 © 2014 IEEE

IEEE photonics SOCIETY

IEEE

Multimode Fiber Coupled Superconductor Nanowire Single-Photon Detector

Labao Zhang, Ming Gu, Tao Jia, Ruiyin Xu, Chao Wan, Lin Kang, Jian Chen, and Peiheng Wu

School of Electronic Science and Engineering, University of Nanjing, Nanjing 210093, China.

DOI: 10.1109/JPHOT.2014.2360285

Manuscript received August 1, 2014; revised September 3, 2014; accepted September 9, 2014. Date of publication September 25, 2014; date of current version October 10, 2014. This work was supported in part by the National Natural Science Foundation of China under Grant 61101012, by the National Basic Research Program of China under Grant 2011CBA00202, and by the National Key Scientific Instrument and Equipment Development Projects under Grant 11227904. Corresponding author: L. Zhang (e-mail: lzhang@nju.edu.cn).

Abstract: High-performance superconductor nanowire single-photon detectors (SNSPDs) coupled by 50-μm multimode fiber were designed and fabricated for the purpose of space applications. Microlens coupling between multimode fiber and detector chip was proposed, resulting in coupling efficiency of 86% at the chips with detection area of 15×15 μm^2. An optical structure for enhancing the photons absorption and superconductor nanowires with low critical current of 3 μA were fabricated on the chips. A cryogenic amplifier was adopted to increase the signal-to-noise ratio and time jitter of output pulse. The SNSPD exhibited system efficiency (1550 nm) of 56% at a dark count rate of 100 cps, 50% at a dark count rate of 5 cps, and 40% at a dark count rate of 1 cps. The time jitter was 46 ps at full-width at half-maximum. The multimode fiber coupling system with high performance will promote its applications in free space.

Index Terms: Photon detector, laser communication, multi-mode fiber, niobium nitride.

1. Introduction

Superconductor Nanowire Single-Photon Detectors (SNSPDs) can be applied in numerous areas, such as quantum information [1], integrated circuit diagnosis [2], depth imaging [3], and bio-fluorescence detection [4], because of their high quantum efficiency [5], low dark count rate [6], and wide spectral responsivity [7]. In practical applications, fiber-coupled systems are typically used to guide photons to the detection area of an SNSPD because fiber-coupled systems feature low background photon noise, considerably lower heat load cryogenic systems, and high stability. Single-mode-fiber-coupled SNSPDs with high efficiency [8]–[10] have been developed and applied in quantum key distribution systems [11].

However, the single-mode fiber coupled SNSPD restricted the viable applications [12], [13]. In the application of fluorescence detection [14], it is difficult to collect the light into a single mode fiber that has a spot $(\sim 9\ \mu\text{m})$ and low divergence angle in practical applications. Other applications in free space, such as laser radars [15] and satellite-based quantum communication [16], suffered the same problem of photon coupling. Developing a multi-mode fiber coupled SNSPD system would enhance the usability in these applications [17].

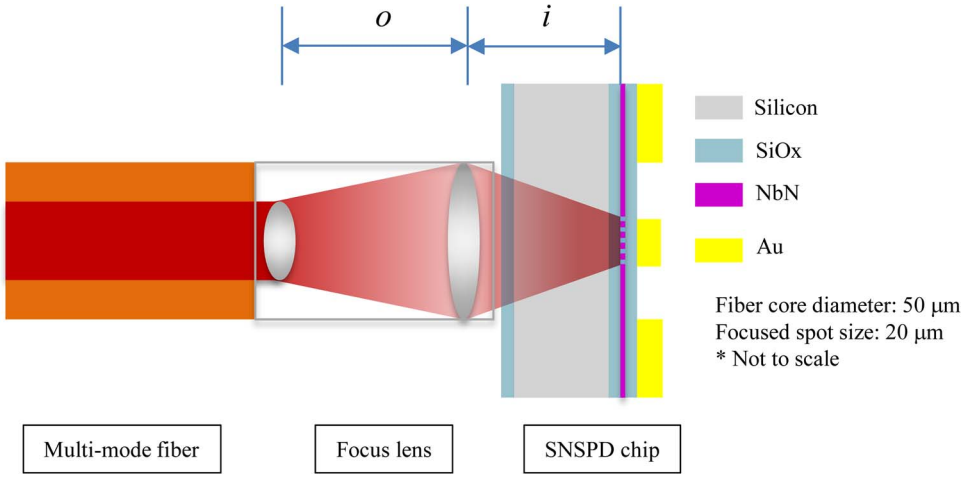

Fig. 1. Schematics of SNSPD chip and its package structure.

Many attempts [18]–[20] tried to increase the detection area for developing multi-mode fiber-coupled SNSPDs. A large active area benefits optical coupling but produces high kinetic inductance, which inevitably degrades the repetition rate of SNSPDs. In addition, the fabrication difficulty increases exponentially as the detection area increases. Therefore the maximum detection area reported thus far is only 40×40 μm^2 [20] for single nanowire, which is smaller than the core diameter (50 μm) of standard multi-mode fibers. Thus, no multi-mode fiber coupled SNSPD with single nanowire has been reported previously. Two multi-mode coupled systems [21]–[23] were developed with SNSPD array covering a large detection area of 66 μm-diameter.

This paper proposes a multi-mode fiber coupled system featuring an improved coupling design and no apparent increase in the detection area of the SNSPD. Micro-lens were coupled to a multi-mode fiber to compress the optical beam. A nominal coupling efficiency of 86% and system efficiency of 56% can be obtained by the chips with detection area of 15×15 μm^2. Optical structure was fabricated to enhance the photons absorption at 1550 nm. At the same time, we reduced the critical current of superconductor nanowire to 3 μA to increase the sensitivity by improved micro-fabrication process, and a cryogenic amplifier was introduced to increase the signal-to-noise ratio and time jitter of output pulse.

2. Design of the Optical Coupling and Package

2.1. Coupling Structure

The optical structure is shown in Fig. 1. The incident beam emitted by the multi-mode fibers was focused using a lens and illuminated the detection area on the back side of the chips.

We first calculated the spot size of the focused beam by first approximation (geometric optics). According to geometric optics theory, the magnification factor is 0.4 with object distance $(o = 7$ mm$)$, image distance $(i = 2.8$ mm$)$, and the confocal length $(f = 2$ mm$)$ of the lens. Thus, the imaging size (focused beam) was 20 μm in diameter estimated for the core (diameter: approximately 50 μm) of multi-mode fibers.

A low magnification should be employed to reduce the spot size, and the divergence angle of the optical beam should be considered. Both of the wide divergence angle and long object distance will result in photon loss in Fig. 1. The numerical aperture of the multi-mode fiber was 0.2 in our system, producing a divergence angle of 11.5°. Thus, the diameter of the divergence beam emitted by the multi-mode fiber at a distance of 7 mm was approximately 2.8 mm, which is lower than that of a lens (approximately 3 mm). In addition, the working distance should be greater than $n_{silicon} \times d$, where d is the thickness of the silicon wafer, as indicated in Fig. 1. In

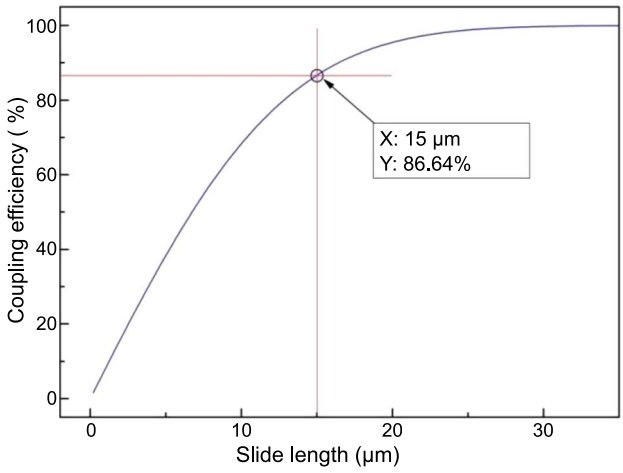

Fig. 2. Nominal coupling efficiency versus slide length of the detection area with the focused beam.

this study, the working distance as the calculated structure was approximately 2.8 mm, which is greater than $n_{silicon} \times d$. Therefore, the optical structure met the requirement for SNSPDs.

2.2. Nominal Coupling Efficiency and Quantum Efficiency

Practical images of a focused beam size are complex because they exhibit aberrations. In this study, we measured the spot size using microscope and a beam profiler. For the paraxial condition, we assumed the beam conform Gaussian distribution according to the approximation resolution of wave equation. The optical distribution was measured by beam profiler and was well fitted with Gaussian function. The diameter D was 20 μm at the beam waist measured by beam profiler, that was consistent with our design and the spot image captured using an infrared camera under a microscope. Beam diameter D was defined to as 4σ, where most photons $(\mathrm{F}(D,\sigma) = 86.47\%)$ were focused in the circle. Then, the standard deviation $\sigma = 5$ μm was inferred based on diameter $D = 20$ μm measured by the beam profiler.

With the focused beam, the coupling efficiency to a square with slide length L from a Gaussian beam can be express as follows:

$$\mathrm{F}(L,\sigma) = 4\left[\int_0^{\frac{L}{2}} \frac{1}{\sqrt{2\pi}\sigma}\exp\left(-\frac{x^2}{2\sigma^2}\right)dx\right]^2. \tag{1}$$

The integration in (1) has no analytical solution; therefore, the numerical method was used to calculate the nominal coupling efficiency of the detection area using (1), as indicated in Fig. 2.

As indicated in Fig. 2, the nominal coupling efficiency increased as the slide length of the detection area increased; however, as mentioned previously, increasing the detection area increases the fabrication difficulty and reduces the repetition rate. Therefore, a detection area of 15×15 μm^2 was adopted in this experiment. As indicated in Fig. 2, the nominal coupling efficiency of the 15×15 μm^2 detection area reached 86.6% based on the proposed coupling settings.

2.3. Chip Fabrication

The chips were fabricated using a standard process as reference [19]. Anti-reflection layers of 269 nm were grown on both sides of a silicon wafer through thermal oxidation to reduce the reflection loss at the interface. An approximately 4-nm-thick NbN layer was deposited on the SiOx

surface through reactive sputtering. The critical temperature of the 4 nm NbN film was 7.8 K. Subsequently e-beam lithography and reactive ion etching were applied to fabricate 50-nm NbN superconductor nanowires with a gap of 50 nm, which covered the 15×15 μm^2 detection area. Another oxide silicon layer with a thickness of 250 nm was then grown on the detection area by PECVD at 370 K. The index of oxide silicon grown through thermal oxidation was 1.44, and the index of the oxide silicon grown by PECVD was 1.55. The thickness and index of oxide silicon layers were measured by step profiler and spectrometer. Finally, a 120-nm-Au mirror was fabricated on the oxide silicon film through e-beam evaporation.

The detection area was located in an optical cavity, as indicated in Fig. 1. The absorption spectra of the structure revealed an absorption peak of approximately 85% at 1550 nm by numerical calculation as in [24].

2.4. Measurement Settings

The designed lens and multi-mode fiber were fixed to a copper plate, and the compressed beam was well aligned with the detection area of the SNSPD chip. To avoid alignment deviation caused by heat shrink during cooling, coaxial structure was adopted in the package settings. With the package, focused spot on the detection area illuminated by 1550 nm light from multimode fiber was examined by placing it on low temperature stage (3–300 K) with an optical window monitored by an infrared microscope, and no apparent deviation was observed with the focused spot under 1000$\times$ IR microscope during cooling from 300 K to 3 K.

To detect single photon, the packaged device was installed in a closed-cycle refrigerator, a GM cryo-cooler, that has two cold stages. A pigtail fiber was connected to a standard optical fiber that was linked to the outside of the GM cryocooler to import optical signals in practical applications. The measurement settings were similar to those used in a previous study [6]. However, a cryogenic SiGe low-noise amplifier was used as a preamplifier to increase the signal-to-noise ratio. The cryogenic amplifier exhibited a gain of 30 dB (1–5000 MHz), noise figure $<$ 10 K, and power consumption of 6 mW.

3. Detector Efficiency

The detector efficiency is the most critical performance parameter of a single-photon detector. High efficiency chips were selected according to electrical properties in advance. The resistance of nanowire at room temperature was measured, and the devices with small resistance were eliminated for short-connecting over the nanowire. For 71 chips fabricated on a 2 inch wafer, 63 chips among them have resistances with low relative deviation ($<$ 10%) from the mean value. Then, we also measured the IV curve of the screened chips at 4.2 K and selected the chips with high critical current and low hysteresis current in the IV curves according to our experience.

The selected samples featured a critical current of approximately 3 μA (at 2.3 K). With the chips and measurement settings, we analyzed the detector efficiency. Theoretically, the system efficiency consists of the coupling efficiency (η_{cf} the probability that the photons were coupled to the detection area), absorption efficiency (η_{af} the probability that the photons were absorbed when coupled to the detection area) and quantum efficiency (η_{qf} the probability that the absorption of one photon in a nanowire results in a response pulse), as follows: $\eta_{sf} = \eta_{cf} \times \eta_{af} \times \eta_{qf}$.

3.1. System Efficiency and Dark Count Rate

The system efficiency (η_{sf}) was adopted to characterize the system performance, which was defined as the ratio of the counting rate to the photon number from the multi-mode fiber. A pico-pulsed laser at 1550 nm and several CW laser diodes at other wavelengths were adopted for the characterization of system efficiency and response spectra. The photon number feed to multimode fiber was fixed at 10^6 for per second in fiber by variable attenuator monitored by power meter as in [19].

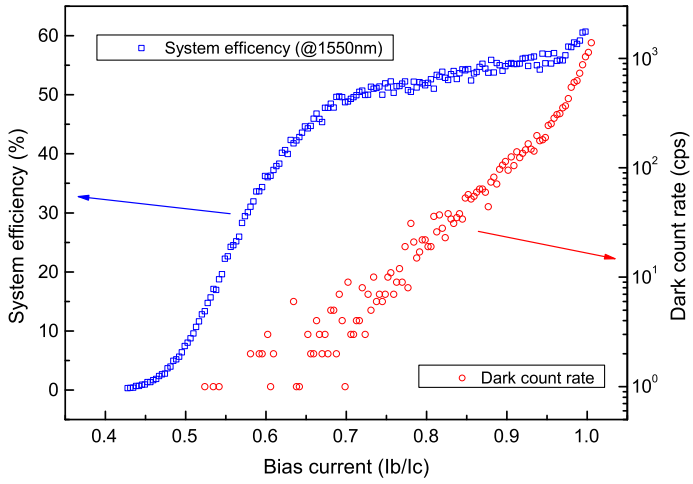

Fig. 3. System efficiency and dark count rate versus bias current.

Fig. 3 shows the system efficiency at 1550 nm and the dark count rate versus the normalized bias current of the proposed SNSPD. The laser pulse repetition rate was set to 10 MHz, and the incident signal was attenuated to 0.1 photons per pulse. Both system efficiency and the dark count rate are the function of bias current as presented in Fig. 3.

As indicated in Fig. 3, the bias current (Ib/Ic) increased both the system efficiency and dark count rate. The system efficiency reached 56% at a dark count rate of 100 cps $(\text{Ib/Ic} = 0.92)$, and 50% at dark count rate of 5 cps $(\text{Ib/Ic} = 0.72)$ as shown in Fig. 3.

As indicated in Fig. 3, the dark count rate was considerably low at various bias currents, which is much lower than those reported in previous study $(\sim 10^6$ cps$)$ [25]. The maximal dark count rate of the proposed SNSPD was only several thousand cps, and it decreased rapidly to approximately 1 cps at $\text{Ib/Ic} = 0.65$, when the system efficiency was still higher than 40%. The dark counts were composed of background light and intrinsic dark counts of the detector. Fiber coupled setting is benefit for avoiding coupling background light. The physics of electrical noise is with debate [26], [27] for complex electrical-thermal interaction over nano-structured device. Semi-empirical results indicate that the chips with uniformed nanowires produce less dark counts [28]. Thus, the low dark count rate was attributed to high quality NbN films of our group [29], reduced bias current and narrow response spectra which filtered the background light as 3.2.

3.2. Response Spectra

The system efficiency at various wavelengths is illustrated in Fig. 4 measured at 0.9 Ib/Ic with the similar method at 1550 nm. In the aforementioned analysis, the system efficiency was determined according to the coupling efficiency, absorption efficiency, and quantum efficiency.

Generally, the quantum efficiency of an SNSPD exhibits a cutoff [30]. When the wavelength is shorter than the cutoff, the quantum efficiency keeps stable, and when the wavelength is longer than the cutoff, the quantum efficiency decreases exponentially as the wavelength increases. The absorption efficiency oscillated over the wavelength, and was enhanced at $d = (2\text{k} + 1)n\lambda/4$ and weakened at $d = \text{k}(n\lambda/2)$, where d is the thickness of the dielectric layer, and k is a positive integer. The coupling efficiency was optimized at 1550 nm where the beam was well focused and aligned at the detection area. The coupling loss increased at other wavelengths, and the coupling efficiency for other wavelength was reduced.

Fig. 4 indicates that the system efficiency increased as the wavelength, and peaked at 1550 nm. High system efficiency was achieved at 1550 nm because high quantum efficiency was maintained, and the absorption efficiency was enhanced. Although the quantum efficiency was high for the

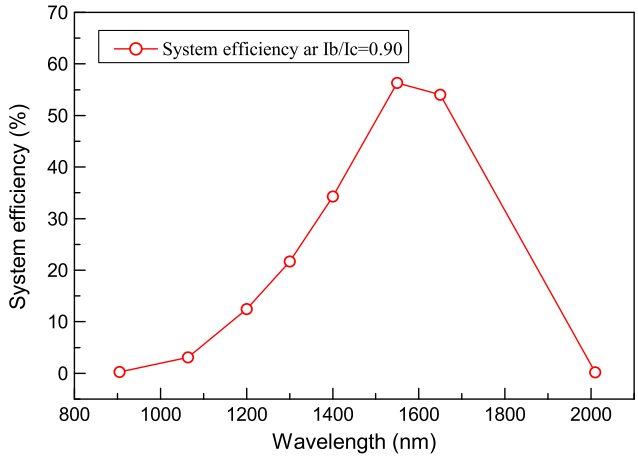

Fig. 4. System efficiency versus wavelength.

photons with wavelength shorter than 1550 nm, the absorption efficiency and the coupling efficiency were was weakened by the cavity structure, thus reducing the system efficiency. At wavelength higher than the cutoff, both quantum efficiency and coupling efficiency decreased, resulting in the system efficiency decreased for the photons with a wavelength of 2010 nm, as shown in Fig. 4.

The high quantum efficiency at 1550 nm is benefit from the reduced critical current. According to previous results [31], there is a cutoff wavelength, below which the photon response is produced by hot spot, and the quantum efficiency is at a high plateau, after which the quantum efficiency is decreased by increasing wavelength exponentially. However, high cutoff will increase the sensitivity at infrared wavelength. According to the hotspot theory, the superconducting nanowire with low critical current increased the cutoff for the superconducting nanowire easier to be broken by infrared photon with lower energy. Thus, the reduced critical current increased the sensitivity of SNSPD at infrared wavelength.

4. Speed and Time Jitter

Fig. 5 presented the output pulse recorded by a 6-GHz real-time oscilloscope. The yellow curve in Fig. 5 presents the response signal of the SNSPD, and the pink curve presents the synchronization signal of the laser pulse.

In Fig. 5, the rise times t_0 and t_1 correspond to the time of the laser pulse and the output pulse of the SNSPD, respectively. The delay of the fiber exhibited a time deviation $(t_1–t_0)$. For the time resolution of the SNSPD, the time deviation exhibited a Gaussian distribution. Therefore, the full width at half maximum (FWHM) of the distribution was defined as the time jitter. The statistical result regarding the fluctuation in time deviation $(t_1–t_0)$ shown in Fig. 5; the average time was shifted to zero to facilitate observation. The FWHM was 46 ps according to the Gaussian fitting.

At the falling edge, the output signal decreased exponentially for kinetic inductance [32] and finally restored to superconducting state. The relaxation time (τ) was 9.6 ns deduced by exponentially fitting at the falling edge in Fig. 5. If we chose 2τ as the minimum recovery time of SNSPD, the maximum repetition rate can be estimated to be approximately 50 MHz.

Superconductor kinetic inductance might cause the speed to degrade when the detection area is increased. The limited detection area produced a high speed, as indicated in Fig. 5.

The time jitter of the proposed SNSPD, which featured a low critical current, was not reduced to improve the signal-to noise ratio by using the cryogenic amplifier. Generally, the time jitter of a device with high critical current is lower than that of a device with a low critical current because the output pulse of a high critical device exhibits a superior signal-to-noise ratio [33], [34].

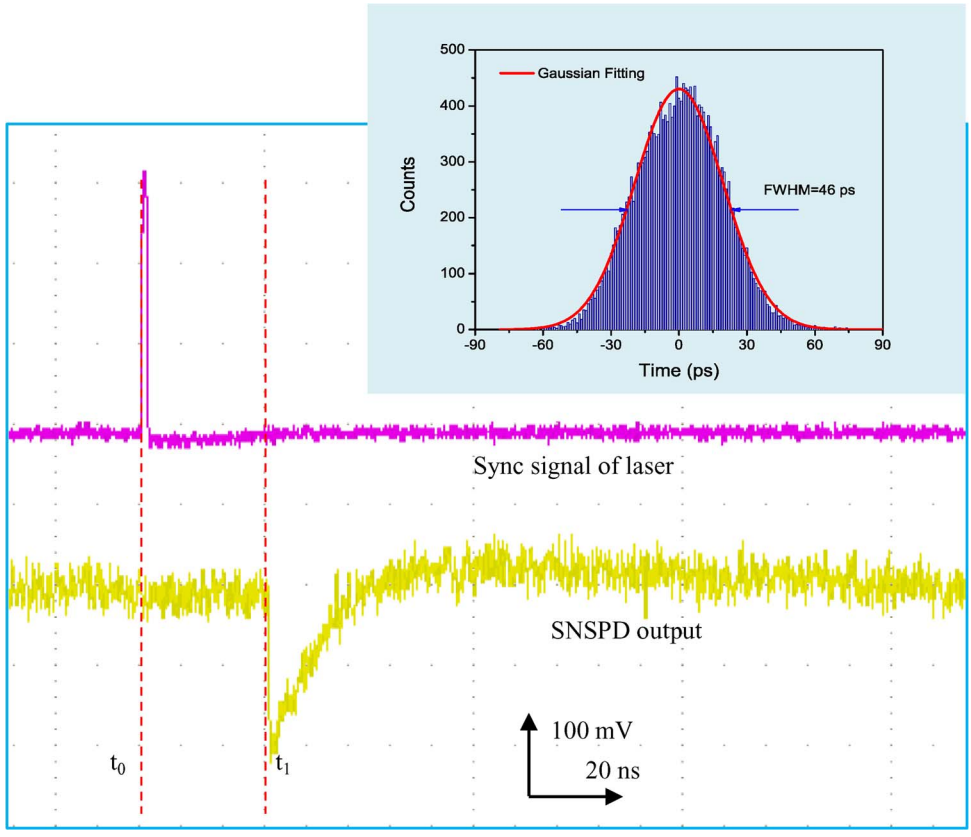

Fig. 5. Output pulse of SNSPD and its arriving time distribution.

Although the critical current was low, the output pulse enabled the signal-to-noise ratio to be similar to those of a previously reported high critical current SNSPD [35], as shown in Fig. 5.

5. Conclusion

In summary, we designed and fabricated a multi-mode fiber coupled SNSPD system that exhibited a system efficiency (1550 nm) of 56% at a dark count rate of 100 cps, 50% at a dark count rate of 5 cps, and 40% at a dark count rate of 1 cps. The time jitter was 46 ps. In addition, the proposed system is sensitive, stable and reliable as traditional SNSPD, and no additional circuit settings are required. Therefore, this system, which features improved multi-mode fiber coupling and high performance, can substantially advance the application of SNSPDs in free space.

References

[1] R. H. Hadfield, "Single-photon detectors for optical quantum information applications," *Nat. Photon.*, vol. 3, pp. 696–705, Dec. 2009.
[2] A. Korneev *et al.*, "GHz counting rate NbN single-photon detector for IR diagnostics of VLSI CMOS circuits," *Microelectron. Eng.*, vol. 69, no. 2–4, pp. 274–278, Sep. 2003.
[3] A. McCarthy *et al.*, "Kilometer-range, high resolution depth imaging via 1560 nm wavelength single-photon detection," *Opt. Exp.*, vol. 21, no. 7, pp. 8904–8915, Apr. 8, 2013.
[4] N. R. Gemmell *et al.*, "Singlet oxygen luminescence detection with a fiber-coupled superconducting nanowire single-photon detector," *Opt. Exp.*, vol. 21, no. 4, pp. 5005–5013, Feb. 25, 2013.
[5] W. H. P. Pernice *et al.*, "High-speed and high-efficiency travelling wave single-photon detectors embedded in nanophotonic circuits," *Nat. Commun.*, vol. 3, pp. 1–10, Dec. 2012.
[6] L. Zhang *et al.*, "Ultra-low dark count rate and high system efficiency single-photon detectors with 50 nm-wide superconducting wires," *Appl. Phys. B-Lasers Opt.*, vol. 102, no. 4, pp. 867–871, Mar. 2011.

[7] F. Marsili *et al.*, "Efficient single photon detection from 500 nm to 5 mu m wavelength," *Nano Lett.*, vol. 12, no. 9, pp. 4799–4804, Sep. 2012.
[8] F. Marsili *et al.*, "Detecting single infrared photons with 93% system efficiency," *Nat. Photon.*, vol. 7, pp. 210–214, Mar. 2013.
[9] D. Rosenberg, A. J. Kerman, R. J. Molnar, and E. A. Dauler, "High-speed and high-efficiency superconducting nanowire single photon detector array," *Opt. Exp.*, vol. 21, no. 2, pp. 1440–1447, Jan. 28, 2013.
[10] S. Miki, T. Yamashita, H. Terai, and Z. Wang, "High performance fiber-coupled NbTiN superconducting nanowire single photon detectors with Gifford-McMahon cryocooler," *Opt. Exp.*, vol. 21, no. 8, pp. 10208–10214, Apr. 22, 2013.
[11] R. H. Hadfield, J. L. Habif, J. Schlafer, R. E. Schwall, and S. W. Nam, "Quantum key distribution at 1550 nm with twin superconducting single-photon detectors," *Appl. Phys. Lett.*, vol. 89, no. 24, pp. 241129-1–241129-3, Dec. 11, 2006.
[12] E. Reiger *et al.*, "Spectroscopy with nanostructured superconducting single photon detectors," *IEEE J. Sel. Topics Quantum Electron.*, vol. 13, no. 4, pp. 934–943, Jul./Aug. 2007.
[13] W. Slysz *et al.*, "Fiber-coupled NbN superconducting single-photon detectors for quantum correlation measurements," *Photon Counting Appl., Quantum Opt., Quantum Cryptogr.*, vol. 6583, pp. 65830J-1–65830J-11, 2007.
[14] A. Tanaka *et al.*, "Noncollinear parametric fluorescence by chirped quasi-phase matching for monocycle temporal entanglement," *Opt. Exp.*, vol. 20, pp. 25228–25238, Nov. 5, 2012.
[15] R. E. Warburton *et al.*, "Subcentimeter depth resolution using a single-photon counting time-of-flight laser ranging system at 1550 nm wavelength," *Opt. Lett.*, vol. 32, no. 15, pp. 2266–2268, Aug. 1, 2007.
[16] C. Z. Peng *et al.*, "Experimental free-space distribution of entangled photon pairs over 13 km: Towards satellite-based global quantum communication," *Phys. Rev. Lett.*, vol. 94, no. 15, p. 150501, Apr. 22, 2005.
[17] W. Slysz *et al.*, "Fiber-coupled single-photon detectors based on NbN superconducting nanostructures for practical quantum cryptography and photon-correlation studies," *Appl. Phys. Lett.*, vol. 88, no. 26, pp. 108–111, Jun. 26, 2006.
[18] S. Miki *et al.*, "Large sensitive-area NbN nanowire superconducting single-photon detectors fabricated on single-crystal MgO substrates," *Appl. Phys. Lett.*, vol. 92, no. 6, pp. 061116-1–061116-3, Feb. 11, 2008.
[19] L. Zhang *et al.*, "Single photon detectors based on superconducting nanowires over large active areas," *Appl. Phys. B-Lasers Opt.*, vol. 97, no. 1, pp. 187–191, Sep. 2009.
[20] F. Mattioli *et al.*, "Large area single photon detectors based on parallel configuration NbN nanowires," *J. Vacuum Sci. & Technol. B*, vol. 30, no. 3, pp. 031204, May/Jun. 2012.
[21] M. E. Grein *et al.*, "A fiber-coupled photon-counting optical receiver based on NbN superconducting nanowires for the Lunar Laser Communication Demonstration," in *Proc. CLEO*, San Jose, California, 2014, p. SM4J.5.
[22] M. Shaw *et al.*, "A receiver for the lunar laser communication demonstration using the optical communications telescope laboratory," in *Proc. CLEO*, San Jose, CA, USA, 2014, p. SM4J.2.
[23] A. Biswas *et al.*, "LLCD operations using the Optical Communications Telescope Laboratory (OCTL)," in *Proc. SPIE*, 2014, pp. 89710X-1–89710X-16.
[24] A. Korneev *et al.*, "Recent nanowire superconducting single-photon detector optimization for practical applications," *IEEE Trans. Appl. Supercond.*, vol. 23, no. 32201204, Jun. 2013.
[25] F. Marsili *et al.*, "High efficiency NbN nanowire superconducting single photon detectors fabricated on MgO substrates from a low temperature process," *Opt. Exp.*, vol. 16, no. 5, pp. 3191–3196, Mar. 3, 2008.
[26] M. K. Akhlaghi, H. Atikian, A. Eftekharian, M. Loncar, and A. H. Majedi, "Reduced dark counts in optimized geometries for superconducting nanowire single photon detectors," *Opt. Exp.*, vol. 20, no. 21, pp. 23610–23616, Oct. 8, 2012.
[27] T. Yamashita *et al.*, "Origin of intrinsic dark count in superconducting nanowire single-photon detectors," *Appl. Phys. Lett.*, vol. 99, pp. 063001-1–063001-16, Oct. 17, 2011.
[28] L. Zhang *et al.*, "Characterization of superconducting nanowire single-photon detector with artificial constrictions," *Aip Advance.*, vol. 4, p. 067114, Jun. 2014.
[29] L. Kang *et al.*, "Suppression of superconductivity in epitaxial NbN ultrathin films," *J. Appl. Phys.*, vol. 109, no, 3, pp. 033908-1–033908-5, Feb. 1, 2011.
[30] A. Korneev, Y. Korneeva, I. Florya, B. Voronov, and G. Goltsman, "Spectral sensitivity of narrow strip NbN superconducting single-photon detector," *Photon Counting Appl., Quantum Opt., Quantum Inf. Transfer Process. III*, vol. 8072, pp. 1–9, May 2011.
[31] A. D. Semenov *et al.*, "Vortex-based single-photon response in nanostructured superconducting detectors," *Phys. C-Supercond. Appl.*, vol. 468, no. 7–10, pp. 627–630, Apr. 1 2008.
[32] A. J. Kerman *et al.*, "Kinetic-inductance-limited reset time of superconducting nanowire photon counters," *Appl. Phys. Lett.*, vol. 88, p. 111116, Mar. 13, 2006.
[33] L. X. You *et al.*, "Jitter analysis of a superconducting nanowire single photon detector," *Aip Adv.*, vol. 3, pp. 1–6, Jul. 2013.
[34] Q. Zhao *et al.*, "Intrinsic timing jitter of superconducting nanowire single-photon detectors," *Appl. Phys. B-Lasers Opt.*, vol. 104, no. 3, pp. 673–678, Sep. 2011.
[35] L. Zhang *et al.*, "A multi-functional superconductor single-photon detector at telecommunication wavelength," *Appl. Phys. B*, vol. 115, no. 3, pp. 295–301, Jun. 1, 2014.